

Identifying Super-Feminine, Super-Masculine and Sex-Defining Connections in the Human Braingraph

László Keresztes^{a,**}, Evelin Szögi^{a,**}, Bálint Varga^a, Vince Grolmusz^{a,b,*}

^a*PIT Bioinformatics Group, Eötvös University, H-1117 Budapest, Hungary*

^b*Uratim Ltd., H-1118 Budapest, Hungary*

Abstract

For more than a decade now, we can discover and study thousands of cerebral connections with the application of diffusion magnetic resonance imaging (dMRI) techniques and the accompanying algorithmic workflow. While numerous connectomical results were published enlightening the relation between the braingraph and certain biological, medical, and psychological properties, it is still a great challenge to identify a small number of brain connections, closely related to those conditions. In the present contribution, by applying the 1200 Subjects Release of the Human Connectome Project (HCP), we identify just 102 connections out of the total number of 1950 connections in the 83-vertex graphs of 1065 subjects, which – by a simple linear test – precisely, without any error determine the sex of the subject. Very surprisingly, we were able to identify two graph edges out of these 102, if, whose weights, measured in fiber numbers, are all high, then the connectome always belongs to a female subject, independently of the other edges. Similarly, we have identified 3 edges from these 102, whose weights, if two of them are high and one is low, imply that the graph belongs to a male subject – again, independently of the other edges. We call the former 2 edges superfeminine and the first two of the 3 edges supermasculine edges of the human connectome. Even more interestingly, one of the edges, connecting the right Pars Triangularis and the right Superior Parietal areas, is one of the 2 superfeminine edges, and it is also the third edge, accompanying the two supermasculine connections, if its weight is low; therefore it is also a “switching” connection.

Running head: Superfeminine & Supermasculine Edges of the Connectome

Keywords: Connectome, braingraph, SVM, linear separation, sex differences,

*Corresponding author

**Joint first authors

Email addresses: keresztes@pitgroup.org (László Keresztes), szogi@pitgroup.org (Evelin Szögi), balorkany@pitgroup.org (Bálint Varga), grolmusz@pitgroup.org (Vince Grolmusz)

superfeminine edges, supermasculine edges

Introduction

One of the most most important challenges in brain science is establishing the cellular and anatomical causes of neurophysiological or psychological differences between human subjects. In the last decade, by the spectacular developments in magnetic resonance imaging (MRI) of the brain, together with the data-processing pipeline for the data collected, our knowledge of the cerebral connections has been increased enormously (e.g., [1, 2, 3]).

Diffusion MRI (dMRI) is capable of discovering the spatial anisotropy of the movement of water molecules in the brain: since in the axonal fibers of the white matter the water molecules have a diffusion movement along the axons, the axonal fibers can be tracked and traced, without any contrast material, with refined tractography algorithms [4]. With the reliable identification of the cortical- and sub-cortical gray matter areas [5], we can construct the connectome, or the braingraph as follows: the nodes (or vertices) of this graph are the anatomically identified gray matter areas, and two nodes are connected by an (undirected) edge if the tractography algorithm finds axonal fibers between the brain areas, corresponding to these two nodes.

Numerous results were published in the last decade, analyzing the human braingraph [6, 7, 8, 9, 10, 11, 12, 13, 14]. Several works describe the connections of the healthy human brain [15, 16, 17, 18, 19, 20, 21, 22], while others establish relations between psychiatric diseases or conditions and the connectome [23, 24, 25, 3, 26, 27].

Sex differences

It is known for several years that the female and the male connectomes have different properties as graphs. The work of [28] has proven – on a publicly un-available dataset – that the ratio of inter-hemispheric connections vs. the intra-hemispheric connections differs in males and females.

Our group has shown on a publicly available dataset [18] that several deep graph-theoretical properties, which are usually applied in the characterization of the quality of large computer interconnection networks [29], are better in the braingraphs of women than in men [30, 31]. We have proven that women’s braingraphs are better expanders, have greater minimal bisection width, more spanning trees, larger minimum vertex cover than that of men. In the work of [32] we have proven that the advantage in the graph-quality parameters of women is due to the sex differences, and not to the size differences: we have compared the graphs of 36 large-brain women and 36 small-brain men, such that the brain volumes of all men were smaller than the brain volume of the smallest-brain woman in the group. We have found that men did not have better parameters than women in this test, and, additionally, many of the advantages of the women remained valid.

Parameters, defined a priori vs. a posteriori

In the studies of [28, 30, 31, 32], the authors compared parameters, which were identified *a priori*, i.e., the examination of these parameters were decided *before* the braingraphs were analyzed. In the present work, we intend to identify *a posteriori* parameters, i.e., edge-structures in the course of the analysis of the braingraphs, in which the male and female connectomes differ. Additionally, we intend to discover the smallest possible edge-sets of the braingraphs, which already determine the sex of the subject.

First we constructed and trained a deep artificial neural network (ANN, see, e.g., [33, 34] for definitions and examples) for classifying the sex of the subject, using only his/her braingraph. While these efforts were moderately successful, we have found that not the deep networks, but, on the contrary, the one level networks gave the best results for predicting the sex of the subject. In a certain sense, one-level neural networks are similar in their capabilities to simple linear test, or Support Vector Machines (SVMs). In the Methods section, we give a short introduction to SVMs.

Few edges, which simply determine the sex of the subject

Applying Support Vector Machines and integer programming algorithms, we were able to identify a small set of connectome edges, which precisely identify the female and male brains; and 2 and 3 particular edges, with the following property: if the fiber number of both edges are high enough, then the connectome belongs to a female subject. If the fiber number of the first two of the three edges are high, and the weight of the third is low enough, then the connectome belongs to a male subject. We call these edges superfeminine and supermasculine edges, respectively.

More exactly, we are considering graphs on 83 vertices. From these 83 vertices, one can form

$$\binom{83}{2} = 3403$$

vertex-pairs, i.e., this is the maximum number of edges on 83 vertices. Note that each of the 1065 braingraphs contains exactly 83 vertices, and all of these vertices correspond to the very same 83 gray-matter areas of the brain (sometimes called ROIs, Regions of Interest). We consider the edges with weights, corresponding to the defining axonal fibers, individually scaled to a number between 0 and 1 (the details are given in the Methods section).

In our dataset of 1065 subjects, the union of all the edges of the 1065 braingraphs contain 1950 edges. That means that out of the possible 3403 edges, only 1950 are present in the union of all the 1065 braingraphs. This is not a surprising observation since few areas from the left hemisphere are connected directly to the areas of the right hemisphere (see Supporting Figure 1 in the on-line supporting material).

If we consider these 1950 edges (or vertex-pairs, if the edge is not present) in any of our 1065 graphs, one can decide the exact identity of the particular braingraph (we note that no two subjects have exactly the same braingraph

with same weights). Therefore, obviously, the set of these 1950 weighted edges defines *any* property of the subjects, including their sex.

Consequently, it is not interesting that all edges define the sex (or other property) of the subject. However, it is a challenge to find the *smallest* possible set of the edges, which still implies the sex of the subject. This small set of connections may carry the most important features, which differentiate the braingraphs of the sexes.

We were able to identify 102 edges, which already determine the sex of the subjects (Fig. 1). Moreover, these edges determine the sex in a very simple, linear way, described below (the method of the identification of these 102 edges is detailed in the Methods section). For describing this phenomenon, let us correspond each graph to a length-102 vector, with coordinates equal to the edge-weights on the chosen 102 edges. This way, we have 1065 vectors, each with 102 coordinates. In other words, we have a 102-dimensional Euclidean space, with 1065 points (vectors) in it. In this space we have determined a hyperplane, which separates the male and female graphs in the following way: all the 102-dimensional vectors, made from the female graphs are on one side of the hyperplane, while all the 102-dimensional vectors, made from the male braingraphs are on the other side of the hyperplane. Consequently, (i) 102 edges out of the 1950 edges already determine the sex of the subject, and (ii) in a very simple, exact, and linear way, by a separating hyperplane. Figure 1 gives a simple example for the data separation on the plane (in 2 dimensions) with a line (i.e., a line is a hyperplane on the plane).

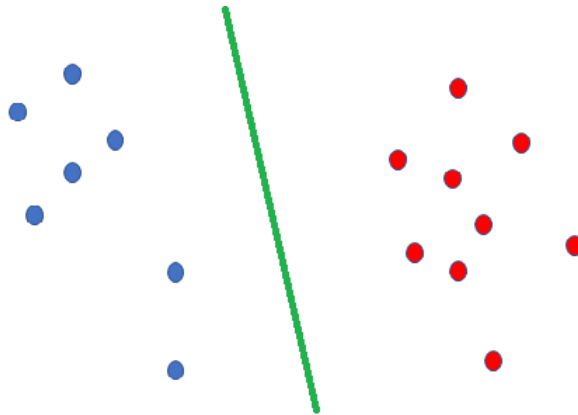


Figure 1: A simple example for Support Vector Machine data classification [35] on the plane. The blue and red points describe two classes of data (for example, each point corresponds to a braingraph, blue points to male, red points to female connectomes). The green line perfectly distinguishes the two classes: the blue ones are on one side, the red ones on the other side of the green line. In the 102-dimensional space (instead of the 2-dimensional space on the figure), we have succeeded to distinguish the male and female braingraphs in a similar way: all the male graphs are on one side, all the female graphs are on the other side of our hyperplane. The coordinates of the separating hyperplane are given in the Supporting material.

Figure 2 depicts the 102 edges, which already determine the sex of the subject. The list of these 102 edges is given in the Supporting Table 1.

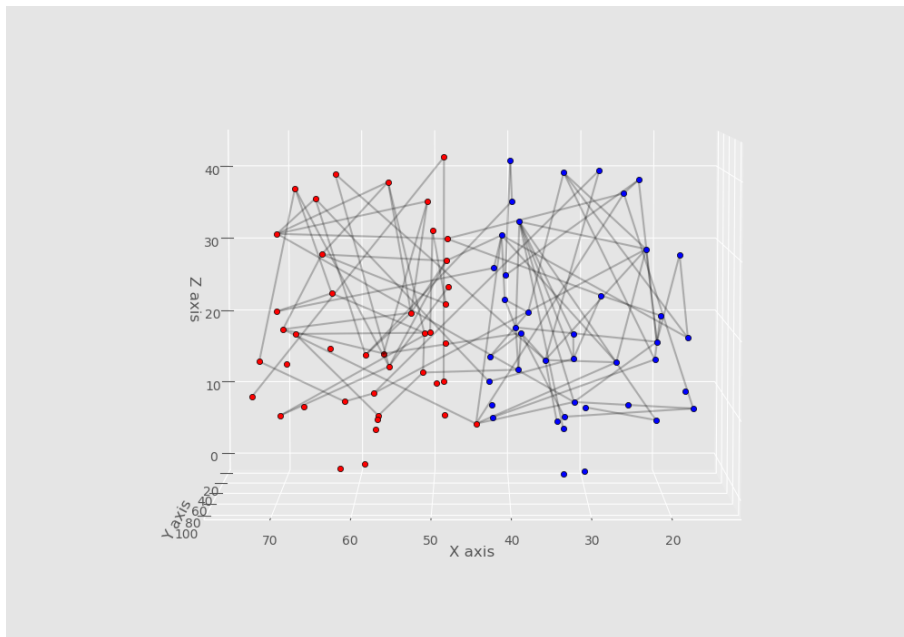


Figure 2: A braingraph of a subject, with 83 vertices and the 102 edges, whose weights (i.e., fiber numbers) already determine the sex of the subject. Labels on the axes are voxel coordinates in mm. In the 102-dimensional space, the male- and female braingraphs are perfectly separated by a hyperplane, similarly as the green line separates the blue and red dots on Figure 1. The nodes from the distinct hemispheres are colored differently. The list of these 102 edges is given in Supporting Table 1 in the supporting material.

Superfeminine and supermasculine edges

Our second main result is the identification of very few connections, out of the 102 edges, in a way that if each of these edges has specific (either high or low) weights, then the sex of the subject is uniquely determined.

Let us recall that the weight of an edge is the number of the axonal fibers found running between its two endpoints in the tractography algorithm, scaled for individual edges to be between 0 and 1 (the details are given in the Methods section).

We have found that if the weights of both edges below are 1, then, independently from the weights of the remaining 100 edges out of the 102 sex-determining connections, the sex of the subject is female:

- F1: (rh.superiorfrontal, Left-Putamen)
- F2: (rh.parstriangularis, rh.superiorparietal)

We call the set of edges F1. F2 “superfeminine” edges.

Similarly, we have found three edges, such that, if the weights of the first two are high and the weight of the third one is low, then, independently of the other edge-weights of the remaining 99 edges out of the 102 connections, the sex of the subject is male:

M1: (lh.rostralmiddlefrontal, Left-Thalamus-Proper)

M2: (Right-Hippocampus, lh.supramarginal)

F2: (rh.parstriangularis, rh.superiorparietal)

The superfeminine and supermasculine edges are depicted on Figure 3.

We call edges M1 and M2 “supermasculine” edges. Note that edge F2 is present in both sets: if the weight of F1 and F2 are high, then it implies that the graph belongs to a female subject, and if the weight of F2 is low, and the weights of M1 and M2 are high, then the graph belongs to a male subject. We call the edge F2 a “switching” edge.

Methods

Graph construction

Our data source is the 1200 Subjects Release of the Human Connectome Project (HCP) [36], available at the <https://www.humanconnectome.org> site. The subjects were healthy adults between 22 and 35 years of age. We have applied the 3T MR diffusion imaging data and processed it with the Connectome Mapper Tool Kit (CMTK) [37].

Our goal was the construction of graphs, or connectomes, which describe the connections between the distinct, anatomically identified cortical and sub-cortical, gray-matter areas of the brain of the subjects. The nodes (or vertices) of our graphs corresponded to the anatomically identified gray matter areas, and we connected two nodes by an edge, if the workflow, described below, found axonal fibers, running between the areas that corresponded to the nodes. We emphasize that the study of the connectome instead of the whole MR image deals with *exclusively* the connections between the gray matter areas and does not take into account the exact orbit of the axonal fibers, running in the white matter of the brain. This way, we can work with graphs, instead of very redundant spatial imagery, gained from the processing of the diffusion MR images. We note that the (mathematical) graph theory, which was established in 1741 by a work of Euler [38], has very rich structures and several of the most complex and deepest proofs and tools in mathematics (e.g., [39, 40, 41]). Therefore, the transition from images to graphs facilitates the application of the well-developed techniques of the (mathematical) graph theory to one of the most complex organs on the Earth, the human brain.

The axonal fibers are discovered from the diffusion MR images by tractography algorithms. Probabilistic tractography was applied, with 1 million streamlines, by using MRtrix 0.2 tractography software. For each subject, the tractography program was run 10 times. In each run, the number of fibers was

determined for each edge. If in any of the ten runs an edge was non-existent, that is, it was not defined by any fiber in the tractography, then that edge was discarded. Next, from these 10 runs, for each edge, the maximum and minimum number of fibers were deleted, and the average of the remaining 8 fiber numbers was assigned to the edge; this number is used as the weight of the edge. This way, the false positive and false negative edges were dealt with, and large errors, leading to the maximum or minimum fiber numbers of an edge, were discarded: they did not influence the average value.

For each subject, 5 graphs, each with resolutions of 83, 129, 234, 463 and 1015 nodes were computed, by applying the CMTK’s implementation of the FreeSurfer suite of programs for parcellation. [5, 42, 4].

The HCP public release contains the data of 1206 subjects. From these, 1113 contained structural scans. Our workflow was successfully completed for the data of 1065 subjects. The resulting graphs, with 5 resolutions for each subject, can be downloaded from the site <http://braingraph.org/download-pit-group-connectomes/>.

In the present work, we apply only the coarsest 83-node resolution, i.e., we consider 1065 graphs of 1065 subjects, each on 83 vertices. We have found 1950 edges by taking the union of the edges of the 1065 braingraphs on 83 vertices.

In braingraph u the edge v is denoted by e_v^u , for $u = 1, 2, \dots, 1065$, $v = 1, 2, \dots, 1950$. The weight of the edge e_v^u , denoted by $w(e_v^u)$, is the average number of axonal fibers found running between its endpoints in the 8 tractography computations.

An edge-specific weight-scaling method

We would like to scale individually the weights of the edges such that all the resulting edge-weights are between 0 and 1, as follows:

$$(1) \quad x_i^\ell := \frac{w(e_i^\ell) - \min_{u=1}^k w(e_i^u)}{\max_{u=1}^k w(e_i^u) - \min_{u=1}^k w(e_i^u)}$$

if the denominator is not zero; otherwise, let x_i^ℓ be zero; $k = 1065$. This way, for each braingraph, and for each edge, the smallest weight is transformed to 0, and the largest (if differs from the smallest) to 1. From now on, we use this scaled weights x_i^ℓ , instead of the original ones. Let $x^\ell = (x_1^\ell, x_2^\ell, \dots, x_s^\ell)$, $s = 1950$.

In other words, for any ℓ , x^ℓ describes a braingraph, with the new, scaled edges as its coordinates.

In what follows, we do not use the superscript ℓ if the meaning of x is clear from the context.

An SVM-based technique with heuristic improvements

The support vector machines (SVMs) are frequently used tools in artificial intelligence to classify the elements of large data sets [35].

Suppose that we have k data points x^1, x^2, \dots, x^k in the n -dimensional Euclidean space \mathbb{R}^n , and a function $f : \mathbb{R}^n \rightarrow \{0, 1\}$. We intend to find an n -dimensional hyperplane, such that (i) one side of the hyperplane contains all x^i 's with $f(x^i) = 1$, and the other side of the hyperplane contains all x^j 's with $f(x^j) = 0$ (ii) and the hyperplane separates the data points with the largest margin, that is, the distance of the closest data point to the hyperplane is maximized.

If $n \geq k$ then the requirement (i) can always be met (one can see this simply by solving a linear systems of equations for finding the normal vector of the hyperplane). If $n < k$, then (i) (i.e., the perfect separation with a hyperspace) is not always satisfiable. We refer to Cover's theorem for probability estimations for the satisfiability of (i) when $n < k$ [43].

In the present work, first we solved (i) and (ii) for the $n = 1950$ dimensional space, with $k = 1065$, by using the Python Scikit-Learn suite. Next, we intend to reduce the coordinates (i.e., the number of edges), which are present in the separation. In other words, we needed to find as few coordinates as possible, such that the male and female connectomes can be separated by a hyperspace, using only the chosen coordinates.

This goal can be formalized as follows:

Let $\|w\|_0$ denote the number of the non-zero coordinates of vector w . Then we need to find

$$(2) \quad \min \|w\|_0,$$

satisfying

$$(3) \quad w \cdot x + b \geq 0 \text{ for all } x,$$

corresponding to a female braingraph, and

$$(4) \quad w \cdot x + b < 0 \text{ for all } x,$$

corresponding to a male braingraph.

By the best of our knowledge, no optimization method is known for solving this problem exactly in polynomial time. Here we have applied the combination of two simple heuristic solution methods, by which we were able to reduce $\|w\|_0$ from 1950 to 102. In other words, we can identify 102 coordinates of x or, equivalently, 102 edges of the graph, such that the sex of the corresponding subject can be expressed by the sign of the linear expression $w \cdot x + b$. The value of b and the 102 non-zero coordinates of w are given in the Supporting material, in Supporting Table 2.

The first heuristic algorithm is a Weight-Based Dimension-Reduction Algorithm (WBDR): Here, we start with a w , which separates linearly, and next delete of the smallest weight coordinates of w . A rate parameter r defines that the r fraction of the smallest coordinates needs to be deleted. If the new w does

not separate, then we backtrack and decrease r . The code of the algorithm is given in the Supporting Material, as Program Code 1.

The second procedure is a Single Dimension Deleting Algorithm (SDDA): Here we start with a separating w , and take a random order of the non-zero coordinates of w , and attempt to delete one dimension if the separation property remains valid. If not, then we try to delete the next dimension. The code of SDDA is given as Program Code 2 in the Supporting Material.

With the application of the three heuristic algorithms (WBDRA, SDDA, DDDA), we have succeeded in reducing the $\|w\|_0$ to 102.

We need to add that we cannot prove the optimality of the 102-dimensional solution: we think that even better results can be reached. However, by using Cover's theorem [43], the probability that randomly 0-1 labeled $k = 1065$ points are separable by a hyperplane in 102 dimensions is much less than 2^{-100} .

Finding Superfeminine and Supermasculine Edges

Our goal is to identify edges, which have the greatest impact to the decisions (3) and (4). These edges may have very important roles in the sex-specific development and functioning of the human brain. Simply stated, the most important edges would have the coordinates with the largest absolute values in vector w in (3) and (4). In what follows, we formally define 0-generator and 1-generator coordinates for a given function $f : [0, 1]^N \rightarrow \{0, 1\}$.

Let $[N]$ denote the set $\{1, 2, \dots, N\}$.

For $y \in [0, 1]^N$ and $I \subset [N]$ let $y|_I \in [0, 1]^N$ denote:

$$y|_I(j) = \begin{cases} y_j & \text{if } j \in I \\ 0 & \text{otherwise.} \end{cases}$$

Let \mathcal{G} denote the set of our 1065 braingraphs, each represented by an $x \in [0, 1]^N$; originally, $N = 1950$, i.e., each braingraph was represented by a 1950 weighted edges. In the previous section, we have seen that we can reduce $N = 102$.

For an $I \subset [N]$ let $\mathcal{G}|_I := \{x|_I : x \in \mathcal{G}\}$.

Definition 1. We say that $I \subset [N]$ is a 1-generator for f with a seed $x \in [0, 1]^N|_I$, if $\forall y \in \mathcal{G}|_{[N]-I}$ $f(x + y) = 1$. Similarly, we say that $I \subset [N]$ is a 0-generator for f with a seed $x \in [0, 1]^N|_I$ if $\forall y \in \mathcal{G}|_{[N]-I}$ $f(x + y) = 0$

In other words, the seed values in the coordinates in the 0-generator or 1-generator I already determine the value of our f .

Our goal is finding the smallest 0- and 1-generators for f , where f gives the sex of the subject: $f(x) = 0$ for males, and $f(x) = 1$ for females:

$$f(x) = \begin{cases} 1 & \text{if } w \cdot x + b \geq 0 \\ 0 & \text{if } w \cdot x + b < 0 \end{cases}$$

For this f , finding the minimal 0- and 1-generators is essentially a version of a knapsack problem, solvable by integer programming methods. For the reduction, we need some definitions and simple statements:

Definition 2. Let $z_F \in [0, 1]^N$ be defined

$$z_F(i) = \begin{cases} 1 & \text{if } w_i \geq 0 \\ 0 & \text{if } w_i < 0 \end{cases}$$

Let $z_M \in [0, 1]^N$ be defined

$$z_M(i) = \begin{cases} 1 & \text{ha } w_i \leq 0 \\ 0 & \text{ha } w_i > 0 \end{cases}$$

It is easy to see that $x = z_F$ maximizes and $x = z_M$ minimizes $w \cdot x + b$.

We show the reduction for 1-generators, for 0-generators a similar reduction works.

Lemma 1. If $I \subset [N]$ is a 1-generator for f with seed $x \in [0, 1]^N|_I$ then it is also a 1-generator with seed $z_F|_I$

Proof. Let $y \in \mathcal{G}|_{[N]-I}$, then $w \cdot (z_F|_I + y) + b \geq w \cdot (x + y) > 0$. \square

The next Corollary is obvious:

Corollary 2. If I the smallest 1-generator with any seed then it is also the smallest 1-generator with seed $z_F|_I$. \square

Lemma 3. Let ξ_i denote the coordinates of the 0-1 characteristic vector of set I : $\xi_i = 1$ if and only if $i \in I$. Then I is a 1-generator for f with a seed $z_F|_I$ if and only if $\forall x \in \mathcal{G}$, $f(x) = 0$ implies $\sum_{i=1}^N \xi_i \cdot w_i(z_F(i) - x_i) > -w \cdot x - b$.

Proof.

$$(5) \quad \sum_{i=1}^N \xi_i \cdot w_i(z_F(i) - x_i) + w \cdot x + b = w \cdot (z_F|_I + x|_{[N]-I}) + b$$

is non-negative. \square

Note that for any $x : f(x) = 1$ (5) is also non-negative.

From Lemma 3, the optimization problem, which gives the minimum 1-generator, can be written: Minimize $\sum_{i=1}^N \xi_i$, with the condition

$$\sum_{i=1}^N \xi_i \cdot w_i(z_F(i) - x_i) > -w \cdot x - b.$$

We call the edges in 1-generators, where the corresponding seed coordinates are ones, superfeminine edges. We call the edges in 0-generators, where the corresponding seed coordinates are ones, supermasculine edges.

The distinction of by the seed-coordinates are made since the weights correspond to fiber numbers, and the ‘‘strong’’ graph edges, defined by many fibers,

are called superfeminine or supermasculine edges. The superfeminine and supermasculine edges are depicted on Figure 3.

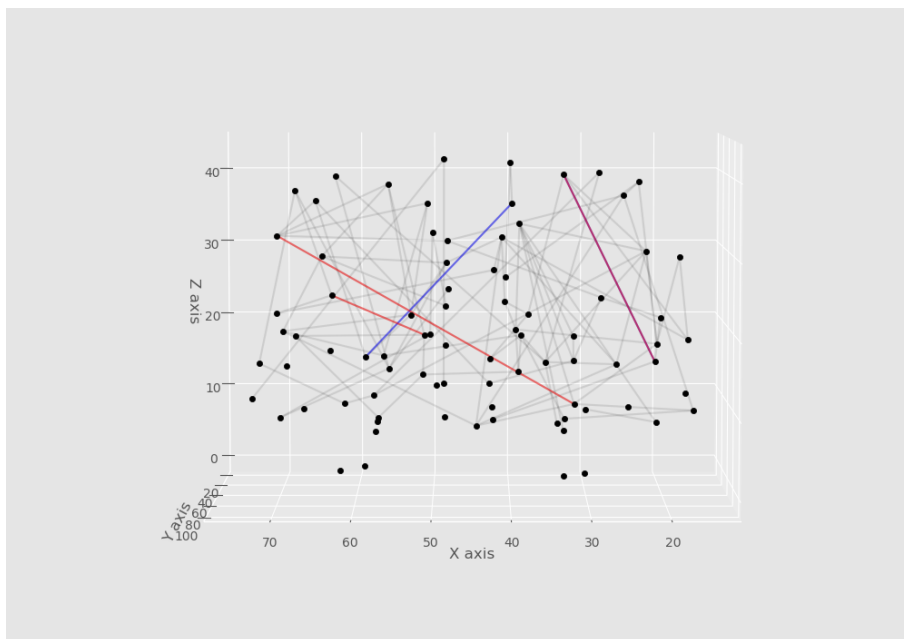


Figure 3: The superfeminine (blue) and supermasculine (red) edges. The switching edge is colored by purple.

Software used

The braingraphs were computed by using the CMTK suite [37], with the details given in the beginning of the section. The figures were created by using Python Matplotlib mplot3D and Networkx packages. The 1950-dimensional SVM was computed using the Python Scikit-Learn suite of programs. The heuristic improvements, resulting in the 102-dimensional separation, were found by the programs given in the Supporting Material in the Program codes section. For IP optimization we used the Python Pulp package.

Discussion and results

Most cerebral sex dimorphisms studies to date were done on very small (up to 40-80 subjects) cohorts and applied mostly volumetric studies [44, 45, 46, 47]. Our previous works [30, 31, 32, 48, 49, 50] first demonstrated sex dimorphisms in *a priori* defined graph parameters, in most cases the better connectivity-related parameters were found in the female connectomes.

Here we first demonstrate relatively small edge-sets, which determine the sex of the subjects on a very large, 1065-member cohort.

The 102 edges, which already define the sex of the subjects are listed in the Supporting material as Supporting Table 1. Obviously, numerous edges connect subcortical nuclei with other parts of the brain. 13 of these 102 edges are inter-hemispheric.

The most frequently appearing nodes in these 102 edges, without considering lateralization, are the inferiorparietal (10 times), posteriorcingulate (9 times), precuneus (9 times), superiorparietal (8 times).

It is known that the inferior parietal lobule, which is a part of the hetero-modal association cortex (HASC), shows sexual volumetric dimorphisms [44, 45].

The sex differences in the development in migraine and the role of precuneus were reported in [46] and in mental rotation [47].

Counting with lateralization, the most frequent nodes are the rh.precuneus (7 times), rh.inferiorparietal (6 times), rh.posteriorcingulate (6 times) and the right-pallidum (6 times), all in the right hemisphere.

By the best of our knowledge, we are the firsts showing that not only these nodes of the braingraph, but rather their important connections, listed in the Supporting Table 1, carries substantial sex dimorphisms.

Additionally, we are the firsts to show the existence of superfeminine and supermasculine edges.

The superfeminine edges we have found are

F1: (rh.superiorfrontal, Left-Putamen)

F2: (rh.parstriangularis, rh.superiorparietal).

The two supermasculine edges with the F2 “switching” edge are:

M1: (lh.rostralmiddlefrontal, Left-Thalamus-Proper)

M2: (Right-Hippocampus, lh.supramarginal)

F2: (rh.parstriangularis, rh.superiorparietal)

The most interesting edge is F2, which, with weight = 1, is a superfeminine edge, and with weight = 0, and with M1 and M2 with weights = 1, it implies the male sex of the subject.

The area of Pars Triangularis was related to hormonal (oxytocin and arginine vasopressin) effects in men, and the same hormones to the parietal cortex – instead of Pars Triangularis – in women [51]. It is striking that just this edge, connecting the Pars Triangularis and the Superior Parietal area in the right hemisphere has this distinguished “switching” property.

There exists numerous other sets of edges with the superfeminine and supermasculine property, we demonstrated these since they were the smallest set we have found. We note that ours (F1, F2, and M1, M2) are relative to the 102-edge set, which we have identified as sex-defining ones. We note also that knowing only the weights of F1, F2 or M1, M2 and F1 will not imply the sex in general, only if they are 1,1 or 1,1,0 respectively.

Conclusions

First in the literature, we have followed an “a posteriori” way of search for edges in the human connectome, which determine the sex of the subjects. We have identified 102 edges that determine the sex in a very simple, linear way in a 1065-member cohort. Additionally, also first in the literature, we have found two and three edges, out of the 102 ones, whose weights being properly set, imply the sex of the subject, independently of the other edges in the graph.

Our results were made possible by the novel edge-specific scaling of the weights of the edges, given by the formula (1). This scaling causes the otherwise low-weight edges also to strongly influence the linear tests (3) and (4). This effect is somewhat similar to the very successful relative PageRank protein-network ranking method in our previous work [52], where the low-degree network nodes have got chances to influence the node-ranking vector of the network.

Author contributions:

LK and ES suggested using SVM in finding characteristic edges, performed integer linear programming optimizations and invented the methods of finding very few (i.e., 102) characteristic edges and the superfeminine and supermasculine edges. BV computed the braingraphs from the HCP public data. VG initiated the study, secured funding, analyzed the results, and wrote the paper.

Data availability

The data source of this work was published at the Human Connectome Project’s website at <http://www.humanconnectome.org> [36] as the 1200-subjects public release. The parcellation data, containing the anatomically labeled ROIs, is listed in the CMTK nipyre GitHub repository https://github.com/LTS5/cmp_nipyre/blob/master/cmtklib/data/parcellation/lausanne2008/ParcellationLausanne2008.xls. The braingraphs, computed by us, can be accessed at the <http://braingraph.org/cms/download-pit-group-connectomes/> site.

Acknowledgments

Data were provided in part by the Human Connectome Project, WU-Minn Consortium (Principal Investigators: David Van Essen and Kamil Ugurbil; 1U54MH091657) funded by the 16 NIH Institutes and Centers that support the NIH Blueprint for Neuroscience Research; and by the McDonnell Center for Systems Neuroscience at Washington University. VG and BV were partially supported by the VEKOP-2.3.2-16-2017-00014 program, supported by the European Union and the State of Hungary, co-financed by the European Regional Development Fund, VG by the NKFI-126472 and NKFI-127909 grants of the National Research, Development and Innovation Office of Hungary. LK and ES

were supported in part by the EFOP-3.6.3-VEKOP-16-2017-00002 grant, supported by the European Union, co-financed by the European Social Fund. The authors are indebted to Balázs Szalkai for consultations on this work.

References

- [1] Olaf Sporns, Giulio Tononi, and Rolf Kötter. The human connectome: A structural description of the human brain. *PLoS Computational Biology*, 1(4):e42, Sep 2005. doi: 10.1371/journal.pcbi.0010042. URL <http://dx.doi.org/10.1371/journal.pcbi.0010042>.
- [2] D. C. Van Essen, K. Ugurbil, E. Auerbach, D. Barch, T E J. Behrens, R. Bucholz, A. Chang, L. Chen, M. Corbetta, S. W. Curtiss, S. Della Penna, D. Feinberg, M. F. Glasser, N. Harel, A. C. Heath, L. Larson-Prior, D. Marcus, G. Michalareas, S. Moeller, R. Oostenveld, S. E. Petersen, F. Prior, B. L. Schlaggar, S. M. Smith, A. Z. Snyder, J. Xu, E. Yacoub, and W. U-Minn H. C. P Consortium . The human connectome project: a data acquisition perspective. *Neuroimage*, 62(4):2222–2231, Oct 2012.
- [3] Balazs Szalkai, Balint Varga, and Vince Grolmusz. Mapping correlations of psychological and connectomical properties of the dataset of the human connectome project with the maximum spanning tree method. *Brain Imaging and Behavior*, 13(5):1185–1192, feb 2019. doi: <https://doi.org/10.1007/s11682-018-9937-6>.
- [4] J Tournier, Fernando Calamante, Alan Connelly, et al. Mrtrix: diffusion tractography in crossing fiber regions. *International Journal of Imaging Systems and Technology*, 22(1):53–66, 2012.
- [5] Bruce Fischl. Freesurfer. *Neuroimage*, 62(2):774–781, 2012.
- [6] Patric Hagmann, Leila Cammoun, Xavier Gigandet, Reto Meuli, Christopher J. Honey, Van J. Wedeen, and Olaf Sporns. Mapping the structural core of human cerebral cortex. *PLoS Biol*, 6(7):e159, Jul 2008. doi: 10.1371/journal.pbio.0060159. URL <http://dx.doi.org/10.1371/journal.pbio.0060159>.
- [7] Balázs Szalkai, Csaba Kerepesi, Bálint Varga, and Vince Grolmusz. The Budapest Reference Connectome Server v2. 0. *Neuroscience Letters*, 595: 60–62, 2015.
- [8] Csaba Kerepesi and Vince Grolmusz. The Giant Virus Finder discovers an abundance of giant viruses in the Antarctic dry valleys. *Archives of Virology*, 162(6):1671–1676, 2017.
- [9] Patric Hagmann, Patricia E. Grant, and Damien A. Fair. MR connectomics: a conceptual framework for studying the developing brain. *Front Syst Neurosci*, 6:43, 2012. doi: 10.3389/fnsys.2012.00043. URL <http://dx.doi.org/10.3389/fnsys.2012.00043>.

- [10] Balazs Szalkai, Csaba Kerepesi, Balint Varga, and Vince Grolmusz. High-resolution directed human connectomes and the consensus connectome dynamics. *PLoS ONE*, 14(4):e0215473, September 2019. URL <https://doi.org/10.1371/journal.pone.0215473>.
- [11] R Cameron Craddock, Michael P. Milham, and Stephen M. LaConte. Predicting intrinsic brain activity. *Neuroimage*, 82:127–136, Nov 2013. doi: 10.1016/j.neuroimage.2013.05.072. URL <http://dx.doi.org/10.1016/j.neuroimage.2013.05.072>.
- [12] Csaba Kerepesi, Balint Varga, Balazs Szalkai, and Vince Grolmusz. The dorsal striatum and the dynamics of the consensus connectomes in the frontal lobe of the human brain. *Neuroscience Letters*, 673:51–55, March 2018. doi: 10.1016/j.neulet.2018.02.052.
- [13] Balazs Szalkai, Csaba Kerepesi, Balint Varga, and Vince Grolmusz. Parameterizable consensus connectomes from the Human Connectome Project: The Budapest Reference Connectome Server v3.0. *Cognitive Neurodynamics*, 11(1):113–116, feb 2017. doi: <http://dx.doi.org/10.1007/s11571-016-9407-z>.
- [14] A Ortiz, JM Gorriz, Javier Ramirez, and Diego Salas-Gonzalez. Improving MR brain image segmentation using self-organising maps and entropy-gradient clustering. *Information Sciences*, 262:117–136, 2014.
- [15] Gareth Ball, Paul Aljabar, Sally Zebari, Nora Tusor, Tomoki Arichi, Nazakat Merchant, Emma C. Robinson, Enitan Ogundipe, Daniel Rueckert, A David Edwards, and Serena J. Counsell. Rich-club organization of the newborn human brain. *Proc Natl Acad Sci U S A*, 111(20):7456–7461, May 2014. doi: 10.1073/pnas.1324118111. URL <http://dx.doi.org/10.1073/pnas.1324118111>.
- [16] Csaba Kerepesi, Balazs Szalkai, Balint Varga, and Vince Grolmusz. How to direct the edges of the connectomes: Dynamics of the consensus connectomes and the development of the connections in the human brain. *PLoS One*, 11(6):e0158680, June 2016. URL <http://dx.doi.org/10.1371/journal.pone.0158680>.
- [17] Cornelia I. Bargmann. Beyond the connectome: how neuromodulators shape neural circuits. *Bioessays*, 34(6):458–465, Jun 2012. doi: 10.1002/bies.201100185. URL <http://dx.doi.org/10.1002/bies.201100185>.
- [18] Csaba Kerepesi, Balazs Szalkai, Balint Varga, and Vince Grolmusz. The braingraph. org database of high resolution structural connectomes and the brain graph tools. *Cognitive Neurodynamics*, 11(5):483–486, 2017.
- [19] Dafnis Batalle, Emma Muñoz-Moreno, Francesc Figueras, Nuria Bargallo, Elisenda Eixarch, and Eduard Gratacos. Normalization of similarity-based individual brain networks from gray matter MRI and its association with

- neurodevelopment in infants with intrauterine growth restriction. *Neuroimage*, 83:901–911, Dec 2013. doi: 10.1016/j.neuroimage.2013.07.045. URL <http://dx.doi.org/10.1016/j.neuroimage.2013.07.045>.
- [20] Balázs Szalkai, Bálint Varga, and Vince Grolmusz. The robustness and the doubly-preferential attachment simulation of the consensus connectome dynamics of the human brain. *Scientific Reports*, 7(16118), 2017. doi: 10.1038/s41598-017-16326-0.
- [21] Csaba Kerepesi, Balázs Szalkai, Bálint Varga, and Vince Grolmusz. Comparative connectomics: Mapping the inter-individual variability of connections within the regions of the human brain. *Neuroscience Letters*, 662(1): 17–21, 2018. doi: 10.1016/j.neulet.2017.10.003.
- [22] Daniel J. Graham. Routing in the brain. *Front Comput Neurosci*, 8: 44, 2014. doi: 10.3389/fncom.2014.00044. URL <http://dx.doi.org/10.3389/fncom.2014.00044>.
- [23] Federica Agosta, Sebastiano Galantucci, Paola Valsasina, Elisa Canu, Alessandro Meani, Alessandra Marcone, Giuseppe Magnani, Andrea Falini, Giancarlo Comi, and Massimo Filippi. Disrupted brain connectome in semantic variant of primary progressive aphasia. *Neurobiol Aging*, May 2014. doi: 10.1016/j.neurobiolaging.2014.05.017. URL <http://dx.doi.org/10.1016/j.neurobiolaging.2014.05.017>.
- [24] Aaron F. Alexander-Bloch, Philip T. Reiss, Judith Rapoport, Harry McAdams, Jay N. Giedd, Ed T. Bullmore, and Nitin Gogtay. Abnormal cortical growth in schizophrenia targets normative modules of synchronized development. *Biol Psychiatry*, Feb 2014. doi: 10.1016/j.biopsych.2014.02.010. URL <http://dx.doi.org/10.1016/j.biopsych.2014.02.010>.
- [25] Justin T. Baker, Avram J. Holmes, Grace A. Masters, B T Thomas Yeo, Fenna Krienen, Randy L. Buckner, and Dost Öngür. Disruption of cortical association networks in schizophrenia and psychotic bipolar disorder. *JAMA Psychiatry*, 71(2):109–118, Feb 2014. doi: 10.1001/jamapsychiatry.2013.3469. URL <http://dx.doi.org/10.1001/jamapsychiatry.2013.3469>.
- [26] Pierre Besson, Vera Dinkelacker, Romain Valabregue, Lionel Thivard, Xavier Leclerc, Michel Baulac, Daniela Sammler, Olivier Colliot, Stéphane Lehericy, Séverine Samson, and Sophie Dupont. Structural connectivity differences in left and right temporal lobe epilepsy. *Neuroimage*, 100C:135–144, May 2014. doi: 10.1016/j.neuroimage.2014.04.071. URL <http://dx.doi.org/10.1016/j.neuroimage.2014.04.071>.
- [27] Leonardo Bonilha, Travis Nesland, Chris Rorden, Paul Fillmore, Ruwan P. Ratnayake, and Julius Fridriksson. Mapping remote subcortical ramifications of injury after ischemic strokes. *Behav Neurol*, 2014:215380, 2014. doi: 10.1155/2014/215380. URL <http://dx.doi.org/10.1155/2014/215380>.

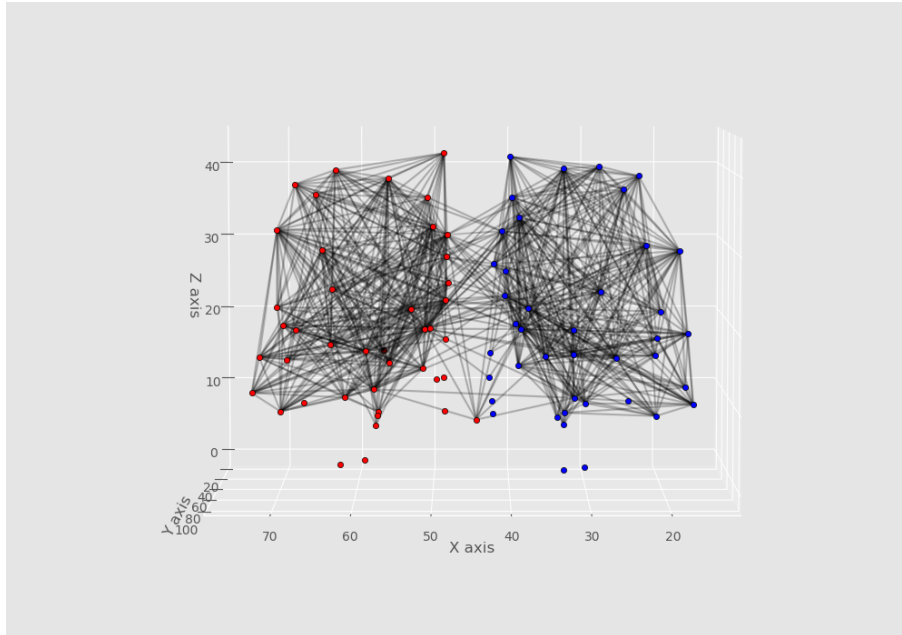
- [28] Madhura Ingalhalikar, Alex Smith, Drew Parker, Theodore D. Satterthwaite, Mark A. Elliott, Kosha Ruparel, Hakon Hakonarson, Raquel E. Gur, Ruben C. Gur, and Ragini Verma. Sex differences in the structural connectome of the human brain. *Proc Natl Acad Sci U S A*, 111(2):823–828, Jan 2014. doi: 10.1073/pnas.1316909110. URL <http://dx.doi.org/10.1073/pnas.1316909110>.
- [29] F Thomson Leighton. *Introduction to parallel algorithms and architectures: Arrays, trees, hypercubes*. Elsevier, 1992. ISBN 9781483221151.
- [30] Balázs Szalkai, Bálint Varga, and Vince Grolmusz. Graph theoretical analysis reveals: Women’s brains are better connected than men’s. *PLoS One*, 10(7):e0130045, 2015. doi: 10.1371/journal.pone.0130045. URL <http://dx.doi.org/10.1371/journal.pone.0130045>.
- [31] Balázs Szalkai, Bálint Varga, and Vince Grolmusz. The graph of our mind. *arXiv preprint arXiv:1603.00904*, 2016.
- [32] Balázs Szalkai, Bálint Varga, and Vince Grolmusz. Brain size bias-compensated graph-theoretical parameters are also better in women’s connectomes. *Brain Imaging and Behavior*, 12(3):663–673, 2018. doi: 10.1007/s11682-017-9720-0. URL <http://dx.doi.org/10.1007/s11682-017-9720-0>.
- [33] Balazs Szalkai and Vince Grolmusz. Near perfect protein multi-label classification with deep neural networks. *Methods (San Diego, Calif.)*, Jul 2017. ISSN 1095-9130. doi: 10.1016/j.ymeth.2017.06.034.
- [34] Balazs Szalkai and Vince Grolmusz. SECLAF: A webserver and deep neural network design tool for hierarchical biological sequence classification. *Bioinformatics*, 2018. URL <https://doi.org/10.1093/bioinformatics/bty116>.
- [35] Corinna Cortes and Vladimir Vapnik. Support-vector networks. *Machine Learning*, 20(3):273–297, 1995.
- [36] Jennifer A. McNab, Brian L. Edlow, Thomas Witzel, Susie Y. Huang, Himanshu Bhat, Keith Heberlein, Thorsten Feiweier, Kecheng Liu, Boris Keil, Julien Cohen-Adad, M Dylan Tisdall, Rebecca D. Folkert, Hannah C. Kinney, and Lawrence L. Wald. The Human Connectome Project and beyond: initial applications of 300 mT/m gradients. *Neuroimage*, 80: 234–245, Oct 2013. doi: 10.1016/j.neuroimage.2013.05.074. URL <http://dx.doi.org/10.1016/j.neuroimage.2013.05.074>.
- [37] Alessandro Daducci, Stephan Gerhard, Alessandra Griffa, Alia Lemkadem, Leila Cammoun, Xavier Gigandet, Reto Meuli, Patric Hagmann, and Jean-Philippe Thiran. The connectome mapper: an open-source processing pipeline to map connectomes with MRI. *PLoS One*, 7(12):e48121, 2012. doi: 10.1371/journal.pone.0048121. URL <http://dx.doi.org/10.1371/journal.pone.0048121>.

- [38] Leonhard Euler. Solutio problematis ad geometriam situs pertinentis. *Commentarii Academiae Scientiarum Imperialis Petropolitanae*, 8(1):128–140, 1741. URL <http://eulerarchive.maa.org/docs/originals/E053.pdf>.
- [39] Endre Szemerédi. Regular Partitions of Graphs. In *Colloq. Internat. CNRS, Univ. Orsay, Orsay, 1976*, volume 260. CNRS, 1975.
- [40] Maria Chudnovsky, Neil Robertson, Paul Seymour, and Robin Thomas. The strong perfect graph theorem. *Annals of Mathematics*, 164(1):51–229, 2006.
- [41] Paul Erdős, Arthur H Stone, et al. On the structure of linear graphs. *Bull. Amer. Math. Soc*, 52(1087-1091):1, 1946.
- [42] Rahul S. Desikan, Florent Ségonne, Bruce Fischl, Brian T. Quinn, Bradford C. Dickerson, Deborah Blacker, Randy L. Buckner, Anders M. Dale, R Paul Maguire, Bradley T. Hyman, Marilyn S. Albert, and Ronald J. Killiany. An automated labeling system for subdividing the human cerebral cortex on mri scans into gyral based regions of interest. *Neuroimage*, 31(3):968–980, Jul 2006. doi: 10.1016/j.neuroimage.2006.01.021. URL <http://dx.doi.org/10.1016/j.neuroimage.2006.01.021>.
- [43] Thomas M Cover. Geometrical and statistical properties of systems of linear inequalities with applications in pattern recognition. *IEEE Transactions on Electronic Computers*, EC-14(3):326–334, 1965.
- [44] Melissa E Frederikse, Angela Lu, Elizabeth Aylward, Patrick Barta, and Godfrey Pearlson. Sex differences in the inferior parietal lobule. *Cerebral Cortex*, 9(8):896–901, 1999.
- [45] Tim Koscik, Dan O’Leary, David J Moser, Nancy C Andreasen, and Peg Nopoulos. Sex differences in parietal lobe morphology: relationship to mental rotation performance. *Brain and cognition*, 69(3):451–459, 2009.
- [46] Nasim Maleki, Clas Linnman, Jennifer Brawn, Rami Burstein, Lino Baccera, and David Borsook. Her versus his migraine: multiple sex differences in brain function and structure. *Brain : a journal of neurology*, 135: 2546–2559, August 2012. ISSN 1460-2156. doi: 10.1093/brain/aws175.
- [47] Tracy Butler, Julianne Imperato-McGinley, Hong Pan, Daniel Voyer, Juan Cordero, Yuan-Shan Zhu, Emily Stern, and David Silbersweig. Sex differences in mental rotation: top-down versus bottom-up processing. *NeuroImage*, 32:445–456, August 2006. ISSN 1053-8119. doi: 10.1016/j.neuroimage.2006.03.030.
- [48] Mate Fellner, Balint Varga, and Vince Grolmusz. The frequent subgraphs of the connectome of the human brain. *Cognitive Neurodynamics*, 13(5): 453–460, 2019. URL <https://doi.org/10.1007/s11571-019-09535-y>.

- [49] Mate Fellner, Balint Varga, and Vince Grolmusz. The frequent network neighborhood mapping of the human hippocampus shows much more frequent neighbor sets in males than in females. *arXiv preprint arXiv:1811.07423*, 2018.
- [50] Máté Fellner, Bálint Varga, and Vince Grolmusz. The frequent complete subgraphs in the human connectome. In *International Work-Conference on Artificial Neural Networks*, volume 11507, pages 908–920. Springer, Springer, 2019.
- [51] Leah H Rubin, Li Yao, Sarah K Keedy, James L Reilly, Jeffrey R Bishop, C Sue Carter, Hossein Pournajafi-Nazarloo, Lauren L Drogos, Carol A Tamminga, Godfrey D Pearson, Matcheri S Keshavan, Brett A Clementz, Scot K Hill, Wei Liao, Gong-Jun Ji, Su Lui, and John A Sweeney. Sex differences in associations of arginine vasopressin and oxytocin with resting-state functional brain connectivity. *Journal of neuroscience research*, 95: 576–586, January 2017. ISSN 1097-4547. doi: 10.1002/jnr.23820.
- [52] Dániel Bánky, Gábor Iván, and Vince Grolmusz. Equal opportunity for low-degree network nodes: a pagerank-based method for protein target identification in metabolic graphs. *PLoS One*, 8(1):e54204, 2013.

Supporting Material

Supporting Figure



Supporting Figure 1: The braingraph of the subject of ID number 100206, with 83 vertices. The nodes from the left hemisphere are colored red, the ones from the right hemisphere are colored blue.

Supporting Tables

Supporting Table 1

Here we list the 102 edges we have identified characterizing the sex of the subjects. The ROIs are named according to the table given in https://github.com/LTS5/cmp_nipype/blob/master/cmtklib/data/parcellation/lausanne2008/ParcellationLausanne2008.xls.

- 1 (rh.precuneus, Right-Hippocampus)
- 2 (rh.caudalmiddlefrontal, Left-Hippocampus)
- 3 (rh.parahippocampal, Right-Thalamus-Proper)
- 4 (rh.parsopercularis, rh.rostralmiddlefrontal)
- 5 (rh.posteriorcingulate, rh.insula)
- 6 (rh.posteriorcingulate, rh.bankssts)
- 7 (lh.paracentral, Left-Accumbens-area)
- 8 (rh.precuneus, rh.pericalcarine)

9 (lh.rostralmiddlefrontal, Left-Thalamus-Proper)
 10 (rh.insula, Right-Pallidum)
 11 (rh.posteriorcingulate, Brain-Stem)
 12 (rh.inferiorparietal, rh.transversetemporal)
 13 (rh.lingual, lh.lingual)
 14 (lh.superiorparietal, Left-Caudate)
 15 (rh.precentral, lh.posteriorcingulate)
 16 (rh.parahippocampal, rh.middletemporal)
 17 (lh.rostralmiddlefrontal, lh.postcentral)
 18 (lh.precuneus, lh.pericalcarine)
 19 (rh.caudalanteriorcingulate, rh.posteriorcingulate)
 20 (lh.parsopercularis, lh.rostralmiddlefrontal)
 21 (lh.fusiform, lh.superiortemporal)
 22 (rh.inferiorparietal, rh.precuneus)
 23 (rh.superiorfrontal, Left-Putamen)
 24 (lh.caudalmiddlefrontal, Left-Pallidum)
 25 (lh.bankssts, Left-Caudate)
 26 (rh.paracentral, rh.cuneus)
 27 (rh.supramarginal, rh.bankssts)
 28 (rh.inferiorparietal, rh.insula)
 29 (rh.precentral, Brain-Stem)
 30 (Right-Hippocampus, Brain-Stem)
 31 (rh.lingual, Right-Thalamus-Proper)
 32 (lh.isthmuscingulate, lh.inferiorparietal)
 33 (rh.lateraloccipital, Right-Putamen)
 34 (lh.isthmuscingulate, lh.precuneus)
 35 (rh.pericalcarine, rh.lingual)
 36 (Right-Hippocampus, lh.supramarginal)
 37 (lh.postcentral, lh.superiortemporal)
 38 (rh.superiorparietal, rh.inferiorparietal)
 39 (lh.superiorparietal, Left-Thalamus-Proper)
 40 (lh.supramarginal, lh.superiorparietal)
 41 (rh.superiorparietal, Right-Caudate)
 42 (rh.middletemporal, Right-Hippocampus)
 43 (lh.pericalcarine, lh.inferiortemporal)
 44 (lh.posteriorcingulate, lh.supramarginal)
 45 (lh.transversetemporal, Left-Thalamus-Proper)
 46 (rh.precentral, rh.middletemporal)
 47 (rh.precentral, rh.postcentral)
 48 (rh.rostralmiddlefrontal, lh.posteriorcingulate)
 49 (rh.isthmuscingulate, rh.pericalcarine)
 50 (lh.superiorparietal, lh.inferiorparietal)
 51 (rh.caudalanteriorcingulate, lh.parsopercularis)
 52 (lh.inferiorparietal, lh.bankssts)
 53 (rh.parstriangularis, rh.parsopercularis)
 54 (rh.insula, Brain-Stem)

55 (rh.precuneus, Right-Putamen)
56 (lh.paracentral, lh.middletemporal)
57 (rh.parstriangularis, rh.superiorparietal)
58 (lh.inferiortemporal, Left-Pallidum)
59 (rh.postcentral, rh.transversetemporal)
60 (lh.caudalanteriorcingulate, Left-Pallidum)
61 (rh.isthmuscingulate, Right-Caudate)
62 (lh.fusiform, Left-Hippocampus)
63 (Left-Caudate, Left-Putamen)
64 (rh.lateralorbitofrontal, Right-Pallidum)
65 (rh.superiorparietal, rh.bankssts)
66 (lh.precentral, Left-Putamen)
67 (lh.bankssts, Brain-Stem)
68 (rh.precuneus, rh.lateraloccipital)
69 (lh.caudalanteriorcingulate, lh.inferiorparietal)
70 (Right-Putamen, Right-Accumbens-area)
71 (lh.lingual, lh.parahippocampal)
72 (Right-Pallidum, lh.caudalmiddlefrontal)
73 (Right-Thalamus-Proper, Right-Pallidum)
74 (rh.superiorfrontal, rh.paracentral)
75 (rh.rostralanteriorcingulate, Right-Thalamus-Proper)
76 (lh.lateraloccipital, lh.bankssts)
77 (lh.caudalanteriorcingulate, Left-Caudate)
78 (rh.supramarginal, rh.transversetemporal)
79 (lh.superiorfrontal, lh.supramarginal)
80 (lh.cuneus, Left-Pallidum)
81 (rh.fusiform, rh.inferiortemporal)
82 (rh.inferiorparietal, Right-Pallidum)
83 (rh.rostralmiddlefrontal, Right-Putamen)
84 (lh.superiorfrontal, lh.lateraloccipital)
85 (rh.medialorbitofrontal, rh.parstriangularis)
86 (lh.precentral, lh.supramarginal)
87 (rh.transversetemporal, Right-Hippocampus)
88 (Right-Thalamus-Proper, lh.lateraloccipital)
89 (rh.posteriorcingulate, lh.caudalanteriorcingulate)
90 (rh.inferiorparietal, Left-Hippocampus)
91 (Right-Accumbens-area, lh.precentral)
92 (rh.pericalcarine, rh.transversetemporal)
93 (lh.parahippocampal, lh.transversetemporal)
94 (rh.posteriorcingulate, rh.isthmuscingulate)
95 (rh.rostralanteriorcingulate, Right-Caudate)
96 (lh.lingual, Left-Thalamus-Proper)
97 (rh.postcentral, rh.cuneus)
98 (rh.caudalmiddlefrontal, Right-Pallidum)
99 (lh.postcentral, Left-Pallidum)
100 (lh.superiorfrontal, Left-Caudate)

101 (rh.precuneus, Right-Amygdala)
102 (rh.precuneus, rh.inferiortemporal)

Supporting Table 2

Here we list the numerical values of the coefficients of the linear expression $w \cdot x + b$, which satisfies

$$w \cdot x + b > 0$$

for all x , corresponding to a female braingraph, and

$$w \cdot x + b < 0$$

for all x , corresponding to a male braingraph.

The number $b = -6.038549870659588237e + 01$. The coordinates of the 102-dimensional vector w , in the same order as the edges are listed in Supporting Table 1:

1 3.140827577736224896e+01
2 -4.224516926777828019e+01
3 -5.534731949947487095e+01
4 -5.021383798706737167e+01
5 3.338868535424175121e+01
6 -6.441754383644450854e+01
7 -9.137204014740284208e+00
8 -1.623199041116811969e+01
9 -1.404986301933692516e+02
10 -4.006330872545306221e+01
11 -4.252783335733649039e+01
12 4.178817508618046617e+01
13 4.372649839601213984e+01
14 4.490601147649471869e+01
15 4.707127337369107067e+01
16 -3.636412443899504154e+01
17 7.015011711412499551e+01
18 4.336665095022959093e+01
19 -7.814457117294969635e+01
20 -4.214089662663334934e+01
21 2.128444054185646195e+01
22 3.312373784233776774e+01
23 1.639952878714990732e+02
24 3.026734348412119502e+01
25 6.268856306230090070e+01
26 -4.715689733082451340e+01
27 2.432515011860931509e+01
28 -3.448165961059984852e+01
29 3.340173045666283969e+01

30 4.042781804276076230e+01
31 2.761020298703500586e+01
32 2.402973906860708198e+01
33 5.799632593673756986e+01
34 2.811207336490517150e+01
35 -3.530994163115634166e+01
36 -1.569561312762774605e+02
37 7.724860503993652117e+01
38 -2.206056231378179433e+01
39 2.931487757932982774e+01
40 -2.102330615674154757e+01
41 2.327980794756512850e+01
42 7.887033703905483151e+01
43 -1.652915811375330790e+01
44 2.233205680678592842e+01
45 -3.287713377723386543e+01
46 3.098515708552118397e+01
47 4.994991466114837664e+01
48 -1.208699629202809689e+01
49 -3.915248510214356514e+01
50 -3.627962519972498256e+01
51 -2.723952954348446909e+01
52 -4.192812642391789524e+01
53 -2.172699471903166213e+01
54 -5.976128513966504840e+01
55 6.259311751749017816e+01
56 3.402550885586439477e+01
57 2.210190354984765690e+02
58 -3.676412998508114072e+01
59 -8.721544084472516545e+01
60 3.913733184781763441e+01
61 3.834602562855815222e+01
62 3.638168347536320368e+01
63 4.718280018698974487e+01
64 3.251867640180642383e+01
65 4.918992981007945531e+01
66 -2.066292878945655787e+01
67 -4.066693930915500488e+01
68 -2.157875932254564333e+01
69 7.650679496763183352e+01
70 4.825588522618672727e+01
71 4.970415751004980365e+01
72 7.295806396686961648e+01
73 -2.882074964324494104e+01
74 3.025214670489702584e+01
75 7.392751412897777641e+01


```

76 3.849139711312415812e+01
77 -2.672208728717341941e+01
78 -7.607620421231430896e+01
79 -6.393366605226245980e+01
80 2.138202760440539052e+01
81 -3.614660559000751761e+01
82 2.635867128635015533e+01
83 7.575343108027709604e+01
84 4.491884096447378738e+01
85 9.919165525049973553e+01
86 2.689606565844382047e+01
87 -4.580873022162855079e+01
88 3.428996344958203935e+01
89 2.134704175565022766e+01
90 -1.729583819036137982e+01
91 5.079962213472451538e+01
92 5.934224772754128452e+01
93 5.915239459823803259e+01
94 1.812222940561209938e+01
95 5.407256405097979979e+01
96 4.579401150729591308e+01
97 7.263014051692987039e+01
98 2.971896563339183928e+01
99 6.289375521391245627e+01
100 -4.140460314388891305e+01
101 -4.235611871509448179e+01
102 4.713752575052093619e+01

```

Program Codes

Program Code 1

```

def drop_by_weight(features, rate=0.2, rate_divisor=1.2):
    tmp_features = features
    while True:
        x_ = x[:, tmp_features]
        clf = LinearSVC(random_state=0, tol=1e-5)
        clf.fit(x_, y)
        y_clf = clf.predict(x_)
        if np.array_equal(y, y_clf):
            features = tmp_features
            w_abs = np.sort(np.abs(clf.coef_[0]))
            threshold = w_abs[int(rate * len(w_abs))]
            tmp_features = [f for f in features if
                np.abs(clf.coef_[0, features.index(f)]) > threshold]
        else:

```

```

        rate_threshold = float(1)/len(features)
    if rate > rate_threshold:
        tmp_features = features
        rate = max(float(rate)/rate_divisor, rate_threshold)
    else:
        break

    return features

```

Program Code 2

```

def drop_one(features):
    while True:
        fl = len(features)
        random.shuffle(features)
        for feature in features:
            clf = LinearSVC(random_state=0, tol=1e-5)
            tmp_features = list(features)
            tmp_features.remove(feature)
            clf.fit(x[:, tmp_features], y)
            y_clf = clf.predict(x[:, tmp_features])
            if np.array_equal(y, y_clf):
                features.remove(feature)
                break
        if len(features) == fl:
            break
    return features

```